

Implications of PREX-2 data on the neutrino-electron scattering in dense matter

Parada T. P. Hutaauruk^{1,*}

¹*Department of Physics, Pukyong National University (PKNU), Busan 48513, Korea*

(Dated: May 9, 2022)

Motivated by the recent measurement of the neutron distribution radius of ^{208}Pb from the PREX-2 data, we study the effects of the new G3(M) parameter set constrained by PREX-2 data on the electron-neutrino scattering in dense matter using the extended relativistic mean field (E-RMF) model. We use the G3(M) parameter set to describe the nuclear matter. The equation of state obtained for the G3(M) parameter set has an excellent agreement with experimental data. We analyze both differential cross section of electron-neutrino and electron-neutrino mean free path to observe their sensitivity to the G3(M) parameter set. We find that the differential cross sections of electron-neutrino for different baryon densities have higher values compared with that obtained for the TM1e and FSU Garnet parameter sets. The higher cross section decreases the electron-neutrino mean free path.

I. INTRODUCTION

Neutrinos play very important role in the evolution processes of the neutron stars and supernova, which the cooling rate of neutron stars (NS), is controlled by neutrinos emission [1, 2]. The neutrinos emission and scattering are sensitive to the equation of state (EOS) of nuclear matter [3–7] and the effective nucleon mass M_N^* [7].

Recently, a measurement of parity violating asymmetry A_{PV} at transferred momentum $q = 0.3978/\text{fm}$ in ^{208}Pb by Lead Radius Experiment (PREX-2) reported an accurate determination of the neutron skin thickness of ^{208}Pb with a precision of approximately equal 1% [8]. Combining analysis of PREX-2 [8] with the PREX previous measurement [9] gives

$$\Delta R_{\text{skin}} = R_n - R_p = (0.283 \pm 0.071) \text{ fm}, \quad (1)$$

where R_n and R_p are respectively the root-mean-squared radii for the neutron and proton density distributions. The accurate measurement of neutron skin thickness ($\Delta R_{np} = R_n - R_p$) is very important and useful tool to constraint the EOS for finite nuclei and nuclear matter. The reliable EOS can be obtained by refitting the appropriate parameters within the theoretical models to reproduce the properties of finite nuclei. The better constraint EOS will lead us to more understanding the properties of neutron stars such as the size, mass and composition and it may affect the electron-neutrino scattering with matter inside the neutron matter or neutron star. Henceforth electron-neutrino is referred simply as “neutrino”.

In the recent works several attempts have analyzed the implications of the PREX-2 data on the EOS [10], symmetry energy [11], and the electric dipole polarizability [12]. In addition the implications of new constraint EOS from the PREX-2 data have been applied to observe the properties of the neutron star [10, 11]. A very recent work of Ref. [10] has developed new parameter set of the E-RMF model through the fine-tuning parameters (Λ_ω which relates with $\eta_{2\rho}$ in our E-RMF model, and g_ρ parameters) to fit the R_n of PREX-2 data [8]. The pa-

rameter set is labeled as the G3(M) parameter set. It was used to validate the constraint from GW170817 binary NS merger to understand the properties of neutron star. The G3(M) parameter set relatively gives a better prediction for finite and nuclear matter. Further detailed explanation of this G3(M) parameter set can be found in Ref. [10]. So far in the literature this G3(M) parameter set are not yet applied to the neutrino scattering with dense matter. It will be very interesting to see how sensitive the EOS and neutrino scattering quantities or observables to the G3(M) parameter set constrained by the accurate measurement of the PREX-2 data [8].

In the present work we perform the extended relativistic mean-field (E-RMF) model with modified G3(M) parameter set [10] constrained by the PREX-2 data [8]. The E-RMF model has been widely use to study the finite nuclei and infinite nuclear matter [13–15]. The predictions of this model are relatively good for describing the bulk properties of finite nuclei at saturation density and properties of neutron star. In this work we calculate the EOS, particle fractions of the constituents of matter which consist of electrons, neutrons, protons and muons, differential cross section (DCRS) of neutrino and neutrino mean free path (NMFP). We then observe the sensitivity of these quantities to the G3(M) parameter set.

We find that the binding energy per nucleon E_B/A for pure nuclear matter (PNM) with the G3(M) parameter set is softer than that obtained for the TM1e [16] and FSU Garnet [17] parameter sets at low baryon density. However, the E_B/A for the G3(M) parameter set is rather stiffer than that obtained for the FSU Garnet parameter set and the same as that obtained for the TM1e parameter set. The pressure for the G3(M) parameter set fits well with the asy-soft of the flow data [18] at intermediate ρ_B/ρ_0 , where ρ_B and ρ_0 are respectively the baryon and saturation densities, but it is in good agreement with the asy-stiff of the flow data [18] at higher ρ_B/ρ_0 . The V_s for the G3(M), TM1e and FSU Garnet parameter sets predict the same speed of sound at saturation density ($\rho_B/\rho_0 \sim 1$) and at $\rho_B/\rho_0 \sim 3.7$.

The total differential cross sections of neutrino for the GM(3) parameter set are found to be higher than that obtained

* phutaauruk@gmail.com

for the TM1e and FSU Garnet parameter sets for different baryon densities. As consequences, the NMFP for the G3(M) parameter set is lower than obtained for the TM1e and FSU Garnet parameter sets.

This paper is organized as follows. In Sec. II we briefly introduce the effective Lagrangian for nuclear matter within the E-RMF model with the G3(M) parameter set. We then calculate the EOS like the energy binding, pressure and speed of sound for pure nuclear matter. In Sec. III we present the formula for both differential cross section of neutrino and neutrino mean free path to observe their sensitivity to the constraint G3(M) parameter set. In Sec. IV our results are presented and their implication are discussed. Sec. V is devoted for a summary.

II. E-RMF MODEL

Here we briefly introduce the equation of state of the matter, which is used to describe the constituents of matter. We use the E-RMF model with the modified G3(M) parameter set, as mentioned already. The effective Lagrangian for the E-RMF model is given by [15, 19]

$$\mathcal{L}_{ERMF} = \mathcal{L}_{NM} + \mathcal{L}_{\sigma} + \mathcal{L}_{\omega} + \mathcal{L}_{\rho} + \mathcal{L}_{\sigma\omega\rho}, \quad (2)$$

where the interaction Lagrangian of the nucleons and mesons is defined by

$$\begin{aligned} \mathcal{L}_{NM} = & \sum_{j=n,p} \bar{\psi} \left[i\gamma^{\mu} \partial_{\mu} - (M_N - g_{\sigma}\sigma) \right. \\ & \left. - \left(g_{\omega}\gamma^{\mu}\omega_{\mu} + \frac{1}{2}g_{\rho}\gamma^{\mu}\tau\cdot\rho_{\mu} \right) \right] \psi, \end{aligned} \quad (3)$$

where the sum stands for the neutrons and protons, M_N are the nucleon masses, and τ are the isospin matrices. The g_{σ} , g_{ω} and g_{ρ} are respectively the coupling constants for the σ , ω and ρ mesons. The m_{σ} , m_{ω} and m_{ρ} are the meson masses. The self-interactions Lagrangian for the σ , ω and ρ mesons are expressed by

$$\begin{aligned} \mathcal{L}_{\sigma} = & \frac{1}{2} \left(\partial_{\mu}\sigma\partial^{\mu}\sigma - m_{\sigma}^2\sigma^2 \right) - \frac{\kappa_3}{6M_N} g_{\sigma}m_{\sigma}^2\sigma^3 \\ & - \frac{\kappa_4}{24M_N^2} g_{\sigma}^2m_{\sigma}^2\sigma^4, \end{aligned} \quad (4)$$

$$\mathcal{L}_{\omega} = -\frac{1}{4}\omega_{\mu\nu}\omega^{\mu\nu} + \frac{1}{2}m_{\omega}^2\omega_{\mu}\omega^{\mu} + \frac{1}{24}\xi_0 g_{\omega}^2(\omega_{\mu}\omega^{\mu})^2, \quad (5)$$

$$\mathcal{L}_{\rho} = -\frac{1}{4}\rho_{\mu\nu}\rho^{\mu\nu} + \frac{1}{2}\rho_{\mu}\rho^{\mu}. \quad (6)$$

The $\omega^{\mu\nu}$ and $\rho^{\mu\nu}$ are the field tensors for the ω and ρ mesons, which are respectively defined as $\omega^{\mu\nu} = \partial^{\mu}\omega^{\nu} - \partial^{\nu}\omega^{\mu}$, and $\rho^{\mu\nu} = \partial^{\mu}\rho^{\nu} - \partial^{\nu}\rho^{\mu}$.

The cross interaction Lagrangian of σ , ω and ρ mesons is

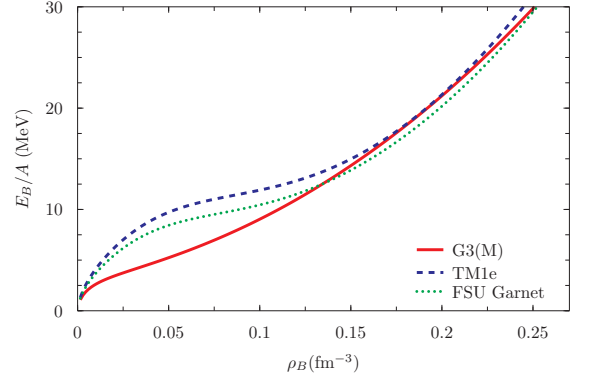


FIG. 1. (color online) Binding energy for pure neutron matter as a function of ρ_B calculated in the E-RMF model for the G3(M) [10] (solid line), TM1e [16] (dashed line) and FSU Garnet [17] (dotted line) parameter sets, where ρ_B is the baryon density.

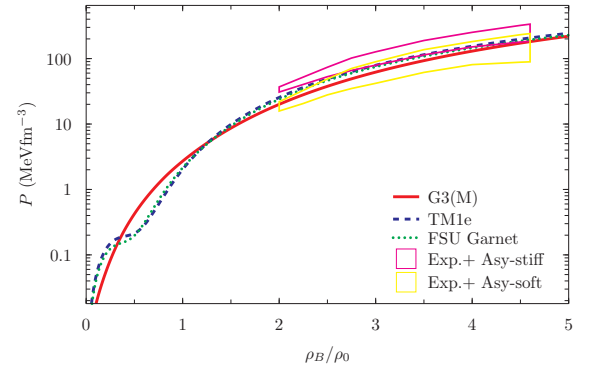


FIG. 2. (color online) Pressure for pure neutron matter as a function of ρ_B/ρ_0 calculated in the E-RMF model using the same parameter sets as used in Fig. 1. The ρ_B and ρ_0 are respectively nucleon and saturation nuclear densities. The line representations are the same as in Fig. 1. The shaded lines are experimental data, which is taken from Ref. [18].

given by

$$\begin{aligned} \mathcal{L}_{\sigma\omega\rho} = & \frac{\eta_1}{2M_N} g_{\sigma}m_{\omega}^2\sigma\omega_{\mu}\omega^{\mu} + \frac{\eta_2}{4M_N^2} g_{\sigma}^2m_{\omega}^2\sigma^2\omega_{\mu}\omega^{\mu} \\ & + \frac{\eta_{\rho}}{2M_N} g_{\sigma}m_{\rho}^2\sigma\rho_{\mu}\rho^{\mu} + \frac{\eta_{1\rho}}{4M_N^2} g_{\sigma}^2m_{\rho}^2\sigma^2\rho_{\mu}\rho^{\mu} \\ & + \frac{\eta_{2\rho}}{4M_N^2} g_{\omega}^2m_{\rho}^2\omega_{\mu}\omega^{\mu}\rho_{\mu}\rho^{\mu}, \end{aligned} \quad (7)$$

where κ_3 , κ_4 , ξ_0 , η_1 , η_2 , η_{ρ} , $\eta_{1\rho}$ and $\eta_{2\rho}$ are the coupling constants. The complete values of the coupling constants in the Lagrangian in Eqs. (3) and (7) are summarized in Table I.

Results for the binding energies per nucleon E_B/A calculated in the E-RMF model for the G3(M), TM1e and FSU Garnet parameter sets are shown in Fig. 1. Figure 1 shows that the energy binding for the G3(M) parameter set is softer at low baryon density compared with the binding energies for the TM1e and FSU Garnet parameter sets. However, at intermediate and high baryon densities, the energy binding for the G3(M) parameter set is rather stiffer than that of for the FSU Garnet parameter set and the same as that of the TM1e

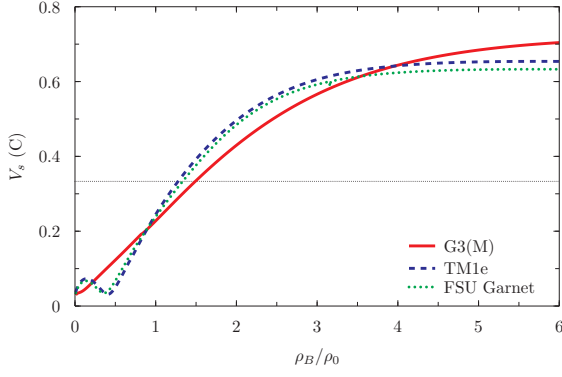


FIG. 3. (color online) Speed of sound V_s as a function of ρ_B/ρ_0 calculated in the E-RMF model using the same parameter sets as used in Fig. 1.

parameter set.

Figure 2 shows the pressure for PNM with the G3(M), TM1e and FSU Garnet parameter sets compared with the experimental data [18]. The pressure for the G3(M) parameter set fits with the asy-soft experimental data [18] at intermediate ρ_B/ρ_0 . However it overlaps with the asy-stiff experimental data [18] at higher ρ_B/ρ_0 .

The speed of sound calculated in the E-RMF model using the G3(M) parameter set is shown in Fig. 3. Compared with the speed of sound for the TM1e and FSU Garnet parameter sets, the G3(M) parameter set has lower speed of sound at intermediate ρ_B/ρ_0 , but higher speed of sound at very lower and higher ρ_B/ρ_0 . All models predict the same speed of sound at saturation density ($\rho_B/\rho_0 \sim 1$) and at $\rho_B/\rho_0 \sim 3.7$, which are crossing points of the models.

III. NEUTRINO SCATTERING IN DENSE MATTER

A. Differential cross section

Based on the weak interaction in the standard model, the Lagrangian density for the neutrino interaction for each constituent of matter is given by the current-current interaction and it has the form [20, 22]

$$\mathcal{L}_{int}^j = \tilde{G}_F [\bar{\nu}\gamma^\mu(1 - \gamma_5)\nu] \left(\bar{\psi}\Gamma_\mu^i\psi \right), \quad (8)$$

where $\tilde{G}_F = \frac{G_F}{\sqrt{2}}$, where $G_F = 1.023 \times 10^{-5}/M_N^2$ and M_N is the nucleon mass. The vertex of the $\Gamma_\mu^j = \gamma_\mu (C_V^j - C_A^j)\gamma_5$ and $j = (n, p, e^-, \mu^-)$ stand for the constituents of matter. For neutron, $C_V = -0.5$ and $C_A = -g_A/2$ and for proton, $C_V = 0.5 - 2\sin^2\theta_w$ and $C_A = g_A/2$, where $g_A = 1.260$ is the axial coupling constant and $\sin^2\theta_w = 0.223$, respectively. For the electron, $C_V = 0.5 + 2\sin^2\theta_w$ and $C_A = 0.5$, and for the muon, $C_V = -0.5 + 2\sin^2\theta_w$ and $C_A = -0.5$. Further details about the values of C_V and C_A can be found in Ref. [6, 20–22].

The neutrino differential cross section is straightforwardly

TABLE I. The complete G3(M) [10] obtained by readjusting to the PREX-2 data [8], TM1e [16] and FSU Garnet [17] parameter sets. The nucleon mass M_N is 939 MeV and all coupling constants are dimensionless. The unit of k_3 is in fm^{-1} .

| Parameters | G3(M) | TM1e | FSU Garnet |
|-----------------|--------|--------|------------|
| m_s/M_N | 0.559 | 0.511 | 0.529 |
| m_ω/M_N | 0.832 | 0.783 | 0.833 |
| m_ρ/M_N | 0.820 | 0.770 | 0.812 |
| m_δ/M_N | 1.043 | 0.980 | 0.000 |
| $g_s/4\pi$ | 0.782 | 0.798 | 0.837 |
| $g_\omega/4\pi$ | 0.923 | 1.004 | 1.091 |
| $g_\rho/4\pi$ | 0.872 | 1.112 | 1.105 |
| $g_\delta/4\pi$ | 0.160 | 0.000 | 0.000 |
| k_3 | 2.606 | -1.021 | 1.368 |
| k_4 | 1.694 | 0.124 | -1.397 |
| β_ω | -0.484 | 0.000 | 0.000 |
| ξ_0 | 1.010 | 2.689 | 4.410 |
| η_1 | 0.424 | 0.000 | 0.000 |
| η_2 | 0.114 | 0.000 | 0.000 |
| η_ρ | 0.645 | 0.000 | 0.000 |
| $\eta_{2\rho}$ | 18.257 | 50.140 | 50.698 |
| α_1 | 2.000 | 0.000 | 0.000 |
| α_2 | -1.468 | 0.000 | 0.000 |
| $f_\omega/4$ | 0.220 | 0.000 | 0.000 |
| $f_\rho/4$ | 1.239 | 0.000 | 0.000 |
| β_σ | -0.087 | 0.000 | 0.000 |

derived from the Lagrangian in Eq. (8) and it gives by [20, 22]

$$\frac{1}{V} \frac{d^2\sigma}{d^2\Omega' dE'_\nu} = -\frac{G_F}{32\pi^2} \frac{E'_\nu}{E_\nu} \text{Im} [L_{\mu\nu}\Pi^{\mu\nu}], \quad (9)$$

with E_ν and E'_ν are the initial and final neutrino energies, respectively. The neutrino tensor $L_{\mu\nu}$ can be defined by

$$L_{\mu\nu} = 8 [2k_\mu k_\nu + (k \cdot q)g_{\mu\nu} - (k_\mu q_\nu + q_\mu k_\nu) - i\epsilon_{\mu\nu\alpha\beta} k^\alpha q^\beta], \quad (10)$$

where the four-momentum transfer is defined as $q = (q_0, \vec{q})$ and k is the initial neutrino four-momentum. The polarization tensor $\Pi^{\mu\nu}$ fro each target particles can be defined by [20, 22]

$$\Pi_{\mu\nu}^j = -i \int \frac{d^4}{(2\pi)^4} \text{Tr} [G^j(p)\Gamma_\mu^j G^j(p+q)\Gamma_\nu^j], \quad (11)$$

where p is the initial four-momentum of the target particles and $G^j(p)$ is the propagator of the target particle j , which is

explicitly can be defined as

$$G^{n,p}(p) = (\not{p}^* M^*) \left[\frac{1}{[p^{*2} = M^{*2} + i\epsilon]} + \frac{i\pi}{E^*} \right] \times \delta(p_0^* - E^*) (p_F^{p,n} - |\vec{p}|), \quad (12)$$

where the $E^* = E + \Sigma_0$ is the effective nucleon energy and $M^* = E + \Sigma_s$ is the effective nucleon mass, where Σ_0 and Σ_s are respectively the scalar and time-like self-energies. The electron and muon propagators are taken the same as the free electron and muon propagators, respectively.

B. Neutrino mean free path

In this section we present the NMFP of the neutrino elastic scattering. The final expression for the inverse NMFP obtained by integrating the differential cross section of Eq. (9) over the energy transfer q_0 and the three component-momentum transfer $|\mathbf{q}|$ at a fixed baryon density can be obtained as [20, 22]

$$\lambda(E_\nu)^{-1} = \int_{q_0}^{2E_\nu - q_0} dq_0 \int_0^{2E_\nu} d|\mathbf{q}| \frac{|\mathbf{q}|}{E'_\nu E_\nu} \frac{2\pi}{V} \frac{d^3\sigma}{d^2\Omega' dE'_\nu}, \quad (13)$$

where the final and initial neutrino energies are related as $E'_\nu = E + q_0$. Further detailed explanations for the determination of the lower and upper limits of the integral can be found in Ref. [20, 22].

IV. NUMERICAL RESULTS

Here our numerical results for the particle fractions of the constituents of matter, differential cross section of neutrino and neutrino mean free path calculated in the E-RMF model for the G3(M) parameter set are presented. The neutrino differential cross section and mean free path are calculated with three component of the four-transferred momentum $|\mathbf{q}| = 2.5$ MeV and initial neutrino energy $E_\nu = 5$ MeV.

Results for the particle fractions of electrons, neutrons, protons, and muons as a function of ρ_B/ρ_0 calculated in the E-RMF model for the G3(M) parameter set are shown in Fig. 4(a) and the particle fractions for the G3(M), TM1e and FSU Garnet parameter sets are shown in Fig. 4(b). The particle fractions of neutrons, protons, and electrons for the G3(M) parameter set have insignificant change with that obtained for the TM1e and FSU Garnet parameter sets, as expected. However, the appearing of muons for the G3(M) parameter set is rather longer than that obtained for the TM1e and FSU Garnet parameter sets, as shown in Fig. 4(b).

Next, the differential cross sections of neutrino calculated in the E-RMF model for the G3(M) parameter set as a function of energy four-transferred momentum q_0 for different baryon

densities (a) $\rho_B = 1.0 \rho_0$ (b) $\rho_B = 2.0 \rho_0$ and (c) $\rho_B = 3.0 \rho_0$ are shown in Fig. 5. The patterns of the differential cross section of neutrino for each constituent change as the baryon density increases. Consequently, it leads to the change of the shape and magnitude of the total differential cross section, as expected.

Compared with total differential cross sections of neutrino for the TM1e and FSU Garnet parameter sets, the G3(M) parameter set has higher value of the cross section as shown in Figs. 6(a)- 6(c). This difference shows the differential cross sections of neutrino are sensitive to the parameter set used. However, in general, the patterns of the differential cross sections of neutrino for different parameters sets are rather the same.

The change of differential cross section of neutrino for each parameter set affects the NMFP as shown in Fig. 7. Figure 7 shows the NMFP for the G3(M) parameter set is lower than that obtained for the TM1e and FSU Garnet parameter sets. However, the NMFP for each parameters set decreases as the ρ_B/ρ_0 increases. Note that the higher NMFP is given by the FSU Garnet parameter set.

V. SUMMARY

To summarize, we have studied the implications of the G3(M) parameter set constrained by PREX-2 data on the equation of state, the particle fractions of the constituents of the matter, differential cross section of neutrino, and NMFP in the E-RMF model.

We find that the binding energy per nucleon for the G3(M) parameter set is softer at low baryon density compared with that obtained for the TM1e and FSU Garnet parameter sets. In contrast, at higher baryon density, the binding energy for the G3(M) parameter set is stiffer than that of and the same as that obtained for the FSU Garnet and TM1e parameter sets, respectively.

Result for the pressure for pure nuclear matter, we find that the pressure for pure nuclear matter for the G3(M) parameter set fits well with the *asy-soft* experimental data at intermediate baryon density. However, at higher baryon density, it has a good agreement with the *asy-stiff* data.

Result for the speed of sound, we find that the speed of sound for the G3(M) parameter set is lower than that of for the TM1e and FSU Garnet parameter sets at intermediate ρ_B/ρ_0 but higher at higher ρ_B/ρ_0 .

We find the differential cross section of neutrino for different densities with the G3(M) parameter set has higher value compared with that obtained for the TM1e and FSU Garnet parameter sets and it decreases the neutrino mean free path.

ACKNOWLEDGMENTS

P.T.P.H. thanks Anto Sulaksono for valuable conversation and Seung-II Nam for useful conversation. This work was supported by the National Research Foundation of Ko-

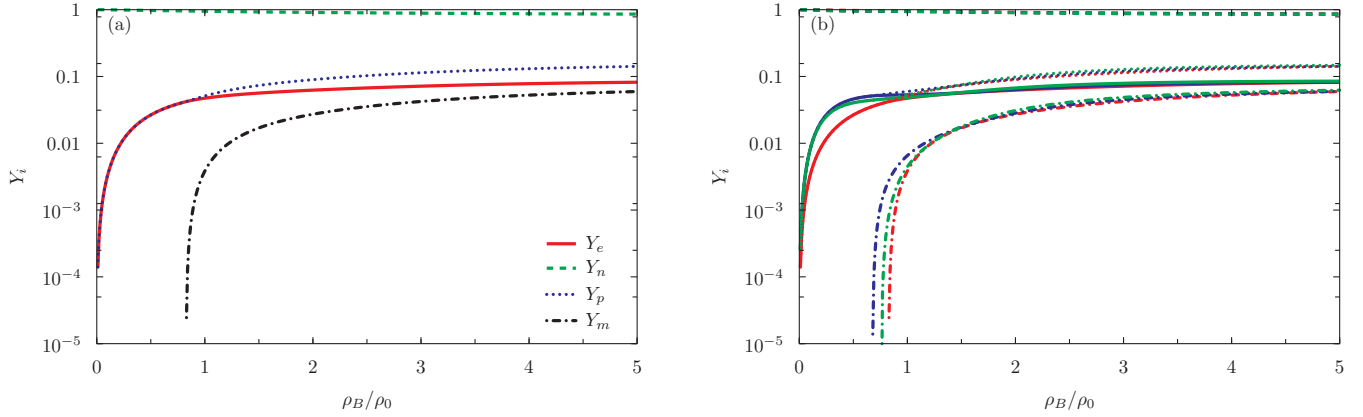


FIG. 4. (color online) Particle fractions of the constituents of the matter as a function of ρ_B/ρ_0 calculated in the E-RMF model for (a) the G3(M) parameters set and (b) for the G3(M), TM1e and FSU Garnet parameter sets which are represented by different colors. The Y_e , Y_n , Y_p , and Y_m represent respectively the electron, neutron, proton and muon fractions.

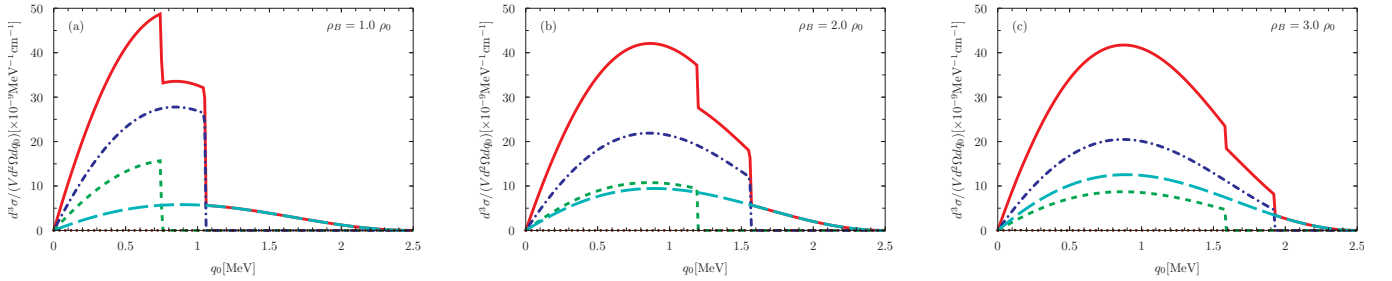


FIG. 5. (color online) Differential cross section of neutrino as a function of q_0 for (a) $\rho_B = 1.0 \rho_0$ (b) $\rho_B = 2.0 \rho_0$ and (c) $\rho_B = 3.0 \rho_0$ calculated in the E-RMF model for the G3(M) parameter set at $|q| = 2.5$ MeV and $E_\nu = 5$ MeV. The solid, dotted-slashed, dashed, long-dashed and dotted lines are the differential cross section of neutrino for total (electrons + neutrons + protons + muons), neutrons, protons, electrons and muon, respectively.

rea (NRF) grant funded by the Korea government (MSIT)

No. 2018R1A5A1025563 and No. 2019R1A2C1005697.

-
- [1] D. G. Yakovlev, A. D. Kaminker, O. Y. Gnedin and P. Haensel, Neutrino emission from neutron stars, Phys. Rept. **354**, 1 (2001).
- [2] A. Burrows and J. M. Lattimer, Neutrinos from SN 1987A, Astrophys. J. Lett. **318**, L63-L68 (1987).
- [3] P. T. P. Hutaruk, A. Sulaksono and K. Tsushima, Effect of neutrino magnetic moment and charge radius on the neutrino mean free path in dense matter with medium modifications of the nucleon form factors, [arXiv:2009.08781 [hep-ph]].
- [4] P. T. P. Hutaruk, Y. Oh and K. Tsushima, Effects of medium modifications of nucleon form factors on neutrino scattering in dense matter, JPS Conf. Proc. **26**, 024031 (2019).
- [5] P. T. P. Hutaruk, Y. Oh and K. Tsushima, Impact of medium modifications of the nucleon weak and electromagnetic form factors on the neutrino mean free path in dense matter, Phys. Rev. D **98**, no.1, 013009 (2018).
- [6] S. Reddy, M. Prakash and J. M. Lattimer, Neutrino interactions in hot and dense matter, Phys. Rev. D **58**, 013009 (1998).
- [7] R. Niembro, P. Bernardos, M. Lopez-Quelle and S. Marcos, Neutrino cross-section and mean free path in neutron stars in the framework of the Dirac-Hartree-Fock approximation, Phys. Rev. C **64**, 055802 (2001).
- [8] D. Adhikari *et al.* [PREX], Accurate Determination of the Neutron Skin Thickness of ^{208}Pb through Parity-Violation in Electron Scattering, Phys. Rev. Lett. **126**, no.17, 172502 (2021).
- [9] S. Abrahamyan, Z. Ahmed, H. Albataineh, K. Aniol, D. S. Armstrong, W. Armstrong, T. Averett, B. Babineau, A. Barbieri and V. Bellini, *et al.* Measurement of the Neutron Radius of ^{208}Pb Through Parity-Violation in Electron Scattering, Phys. Rev. Lett. **108**, 112502 (2012).
- [10] J. A. Pattnaik, R. N. Panda, M. Bhuyan and S. K. Patra, Constraining the relativistic mean-field models from PREX-2 data: Effective forces revisited, [arXiv:2105.14479 [nucl-th]].
- [11] B. T. Reed, F. J. Fattoyev, C. J. Horowitz and J. Piekarewicz, Implications of PREX-2 on the Equation of State of Neutron-Rich Matter, Phys. Rev. Lett. **126**, no.17, 172503 (2021).
- [12] J. Piekarewicz, Implications of PREX-2 on the electric dipole polarizability of neutron rich nuclei, [arXiv:2105.13452 [nucl-th]].
- [13] B. Kumar, S. K. Singh, B. K. Agrawal and S. K. Patra, New parameterization of the effective field theory motivated relativistic

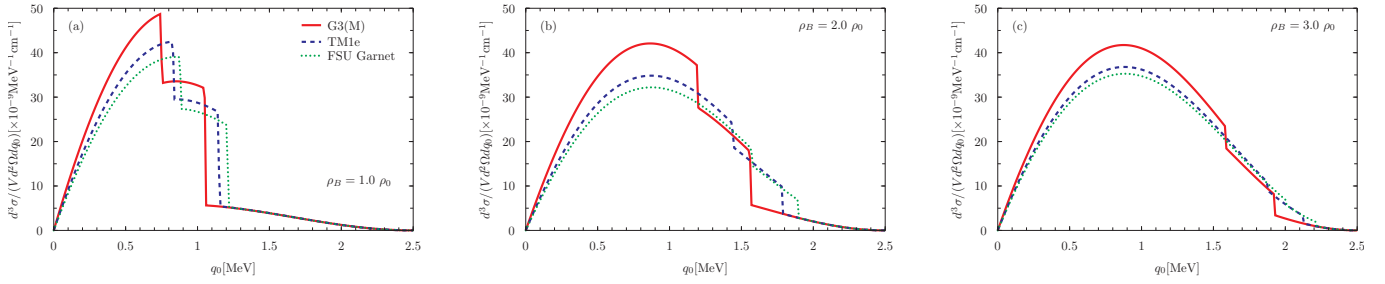


FIG. 6. (color online) Total differential cross section of neutrino as a function of q_0 calculated in the E-MRF model for the same parameters set as in Fig. 1 for (a) $\rho_B = 1.0 \rho_0$ (b) $\rho_B = 2.0 \rho_0$ and (c) $\rho_B = 3.0 \rho_0$.

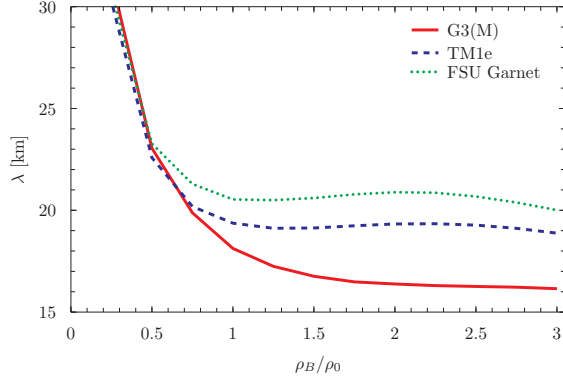


FIG. 7. (color online) NMFP as a function of ρ_B/ρ_0 calculated in the E-RMF model for the G3(M), TM1e and FSU Garnet parameter sets.

mean field model, Nucl. Phys. A **966**, 197-207 (2017).

- [14] B. K. Agrawal, A. Sulaksono and P. G. Reinhard, Optimization of relativistic mean field model for finite nuclei to neutron star matter, Nucl. Phys. A **882**, 1-20 (2012).

- [15] R. J. Furnstahl, B. D. Serot and H. B. Tang, Analysis of chiral mean field models for nuclei, Nucl. Phys. A **598**, 539-582 (1996).
- [16] S. S. Bao, J. N. Hu, Z. W. Zhang and H. Shen, Effects of the symmetry energy on properties of neutron star crusts near the neutron drip density, Phys. Rev. C **90**, no.4, 045802 (2014).
- [17] W. C. Chen and J. Piekarewicz, Searching for isovector signatures in the neutron-rich oxygen and calcium isotopes, Phys. Lett. B **748**, 284-288 (2015).
- [18] P. Danielewicz, R. Lacey and W. G. Lynch, Determination of the equation of state of dense matter, Science **298**, 1592-1596 (2002).
- [19] R. J. Furnstahl, B. D. Serot and H. B. Tang, A Chiral effective Lagrangian for nuclei, Nucl. Phys. A **615**, 441-482 (1997) [erratum: Nucl. Phys. A **640**, 505-505 (1998)].
- [20] A. Sulaksono, P. T. P. Hutaaruk, and T. Mart, Isovector-channel role of relativistic mean field models in the neutrino mean free path, Phys. Rev. C **72**, 065801 (2005).
- [21] P. T. P. Hutaaruk, C. K. Williams, A. Sulaksono, and T. Mart, Neutron fraction and neutrino mean free path predictions in relativistic mean field models, Phys. Rev. C **70**, 068801 (2004).
- [22] C. J. Horowitz and K. Wehrberger, Neutrino neutral current interactions in nuclear matter, Nucl. Phys. A **531**, 665-684 (1991).